An Evaluation of Depth Resolution Requirements for Optical Profiling in Coastal Waters

GIUSEPPE ZIBORDI, DAVIDE D'ALIMONTE, AND JEAN-FRANÇOIS BERTHON

Institute for Environment and Sustainability, Joint Research Centre, Ispra, Italy

(Manuscript received 21 January 2003, in final form 27 November 2003)

ABSTRACT

Wave perturbations induce uncertainties in subsurface quantities determined from the extrapolation of optical measurements taken at different depths. An analysis of these uncertainties was made using data collected in the northern Adriatic Sea coastal waters over a wide range of environmental conditions with a profiling system having a 6-Hz acquisition rate, ~0.1 m s^{-1} deployment speed, radiance sensors with 20° full angle field of view, and irradiance collectors of ~1-cm diameter. The uncertainties were quantified as a function of the depth resolution of radiance and irradiance profiles through the percent differences between the subsurface values computed from full and reduced resolution profiles (the latter synthetically created by removing data from the former). The applied method made the analysis independent from instrument calibration; from perturbations induced by instrument self-shading, deployment structure, and bottom effects; and from environmental variability caused by seawater and illumination changes during casts. The results displayed a significant increase in uncertainties with decreasing depth resolution. For instance, in the 443–665-nm spectral range with a depth resolution of 12.5 cm, the largest uncertainties were observed for the subsurface downward irradiance, $E_d(0^-, \lambda)$, and the near-surface diffuse attenuation coefficient, $K_d(\lambda)$, with spectral average uncertainties of 5.5% and 11.7%, respectively. With the same depth resolution, the smallest uncertainties were observed for the subsurface upwelling radiance, $L_u(0^-, \lambda)$, and upward irradiance, $E_u(0^-, \lambda)$, showing spectral average values of 1.0% and 0.6%, respectively. The uncertainties in the irradiance reflectance, $R(\lambda)$; the Q factor, $Q_n(\lambda)$; and the normalized water-leaving radiance, $L_{WN}(\lambda)$, gave values in keeping with those of the quantities used for their computation. The uncertainties were also analyzed as a function of sea state S_s and diffuse attenuation coefficient K_d at 490 nm. These values were used to estimate the depth resolution requirements restricting below given thresholds the wave-induced uncertainties in the computed subsurface optical quantities. To satisfy a 2% maximum uncertainty in the 443–665-nm spectral range, for the specific instrumental and environmental conditions characterizing the data used in the analysis, results suggested minimum depth resolutions of 11, 40, 3, and 2 cm, for $L_u(0^-, \lambda)$, $E_u(0^-, \lambda)$, $E_d(0^-, \lambda)$, and $K_d(\lambda)$, respectively.

1. Introduction

Radiance and irradiance data have many uses in optical oceanography and remote sensing, being the basis for relationships linking optical properties to seawater constituents. As a result, a variety of fixed-depth optical systems based on buoys (e.g., Clark et al. 1997; Pinkerton and Aiken 1999; Antoine and Guevel 2000) and optical profilers based on winched, crane, and free-fall systems (e.g., Dierssen and Smith 1996; Zibordi et al. 1999; Hooker and Maritorena 2000; Hooker et al. 2003) have been developed. These are regularly used for the collection of optical data in the open ocean and coastal waters to support the development of biooptical algorithms, the validation of remote sensing products, and the vicarious calibration of space sensors when the spatial homogeneity is high around the measurement point.

Subsurface optical quantities at wavelength λ, like upwelling radiance, $L_u(0^-, \lambda)$, upward irradiance, $E_u(0^-, \lambda)$, and downward irradiance, $E_d(0^-, \lambda)$, are commonly extrapolated from $L_u(z, \lambda)$, $E_u(z, \lambda)$, and $E_d(z, \lambda)$ values at different depths z. The basic assumption is that the log-transformed radiometric data linearly decrease with depth (Smith and Baker 1984) in a given near-surface interval hereafter called the extrapolation interval.

A recent theoretical work (Zaneveld et al. 2001) showed that wave effects in the irradiance field, generated by the superimposition of waves with different heights and wavelengths, can significantly perturb the accuracy of the extrapolated subsurface downward irradiance.

The wave effects in each single underwater measurement are intrinsically averaged over the instrument acquisition period, when this is longer than the flash duration, and over the field of view for radiances or the

Corresponding author address: Dr. Giuseppe Zibordi, Institute for Environment and Sustainability, Joint Research Centre, 21020 Ispra, Italy.
E-mail: giuseppe.zibordi@jrc.it

size of the collector for irradiances. For fixed-depth optical systems the perturbations induced by wave effects in subsurface quantities mostly depend on the time interval chosen for the additional averaging of measurements collected at the given acquisition rate for the considered depths. The perturbations in subsurface quantities determined from measurements collected with optical profiling systems depend on the depth resolution defined by the deployment speed and the acquisition rate. Thus, measurements simultaneously taken at the same site with profiling systems having the same optics but different deployment speeds and acquisition rates could lead to the determination of quite different values for the subsurface quantities.

Optical profilers, unlike fixed-depth systems, provide the additional capability of a continuous vertical characterization of the seawater apparent optical properties and the possibility of a cast-by-cast determination of the most appropriate extrapolation interval. The accuracy of subsurface quantities derived from open-ocean optical profiles generally benefits from the absence of significant gradients in the vertical distribution of optically significant components in the upper sea layers. This makes it possible to exclude from the extrapolation interval the profile data largely affected by wave focusing and defocusing in the first few meters below the surface. On the other hand, large gradients in the vertical distribution of optically significant components are a frequent feature of the near-surface layer in coastal waters. These gradients may induce large deviations from linearity of the log-transformed optical data with respect to depth. Thus, the extrapolation of subsurface optical quantities from profiles taken in coastal waters is usually constrained to the very few meters below the surface where the hypothesis of linearity can generally be applied. This significant difference between optical profiles taken in the two marine environments can lead to much larger wave-induced uncertainties in the subsurface quantities determined in coastal waters.

Intuitively, for a given optics any increase in the acquisition rate and decrease in the deployment speed would produce an increase in the accuracy of the subsurface optical quantities due to a more extended averaging of the wave effects over time per unit depth. Commercial instruments like optical free-fall profilers, however, exhibit limitations. Their deployment speed is generally higher than 0.2 m s^{-1}, while the acquisition rate is usually restricted between 6 and 10 Hz.

This work presents and discusses an analysis of the uncertainties affecting subsurface optical quantities as a function of the profile depth resolution for different sea state and seawater attenuation values. The analysis was made using radiance and irradiance profiles collected with a winched system equipped with commercial radiometers and deployed from an oceanographic tower in the northern Adriatic Sea coastal waters. The uncertainties were estimated from differences in the subsurface optical quantities determined from high- and reduced-resolution profiles, with the latter obtained from the former by removing data. The applied method makes the analysis independent from all measurement uncertainties with the exception of wave-induced perturbations, which randomly affect measurements at various depths and then also affect the subsurface values determined from diverse depth resolution profiles.

The objective of this work is to define, for radiance and irradiance profiles taken in coastal waters with a specific class of radiometers, the depth resolution requirements restricting below given thresholds the uncertainties induced by wave perturbations in computed subsurface optical quantities.

2. Background

The focusing and defocusing of sun rays refracted by surface waves produce large light fluctuations in the upper sea layer. The origin, amplitude, frequency, and depth extension of these fluctuations have been addressed both theoretically (e.g., Schenck 1957; Snyder and Dera 1970; Stramski and Dera 1988; Walker 1994; Zaneveld et al. 2001) and experimentally (e.g., Dera and Olszewski 1978; Dera and Stramski 1986; Weidemann et al. 1990; Dera et al. 1993).

Making use of measurements taken at the 525-nm single center wavelength and at a typical fixed depth of ~1 m, Dera and Stramski (1986) showed that the frequency of the so-called light flashes (i.e., fluctuations in intensity exceeding the mean irradiance by a factor of about 1.5) can be higher than 3 Hz, and this frequency exponentially decreases with increasing flash intensity. The most probable duration of flashes was estimated between a few and tens of milliseconds. Additional observations reported by Dera and Stramski (1986) showed a reduction in the fluctuation of irradiance intensity and an increase of flash durations on water depth increase. The wave focusing effects were also been found to be more significant under clear-sky conditions, clear water, low sun zenith, and a relatively smooth water surface driven by a wind speed of 2–5 m s^{-1}. Further relevant result of their work was an analysis of wave effects in the downward irradiance data as a function of the diameter of the collector showing a reduction in fluctuations with an increase in the diameter of the collector in the 2–6-mm range.

Weidemann et al. (1990) addressed the uncertainties in the determination of the diffuse attenuation coefficient from downward irradiance measurements simultaneously taken at fixed depths in a ground tank on controlled water surface perturbations. Upon a wave height increase, results showed uncertainties of up to 30% in the computed diffuse attenuation coefficient. Moving to optical profiles, Zaneveld et al. (2001) presented experimental data and theoretical simulations of wave-induced perturbations in downward irradiance. Their study proposed a method for the determination of the diffuse attenuation coefficient from profile data per-

turbed by waves. The method, suitable for optical profiles taken in the open ocean where the extrapolation interval can be quite extended, is based on the upward integration of the irradiance data starting at a depth at which the irradiance profile is only weakly affected by waves.

3. Measurements

The measurements used in this study were collected within the framework of the Coastal Atmosphere and Sea Time-Series (CoASTS) program (Zibordi et al. 2002) supporting ocean color calibration and validation activities through a comprehensive data collection at the Acqua Alta Oceanographic Tower (AAOT) in the northern Adriatic Sea. The AAOT is positioned 8 n mi offshore of the Venice lagoon (45.314°N, 12.508°E) where the average water depth is approximately 17 m and the sea bottom is mostly composed of sand and mud. A peculiarity of the AAOT is its position in a frontal region characterized by succession of Case-1 and Case-2 waters making the site well representative of coastal zones (here defined as regions permanently or occasionally affected by bottom resuspension, coastal erosion, river inputs, or by relevant anthropogenic impact). The site exhibits an occurrence of roughly 60% Case-1 waters as identified according to Loisel and Morel (1998). However, it must be highlighted that the values defining the Case-1 and Case-2 waters are closely distributed around their separation threshold (Berthon et al. 2002) making their categorization somewhat speculative.

Data relevant to the current study are the in-water optical profiles taken with the Wire-Stabilized profiling Environmental Radiometer (WiSPER) system.

a. WiSPER measurements

WiSPER is a winched system deployed through a custom-built profiling rig with the optical sensors mounted at approximately the same depth and distance (i.e., within a 10-cm relative depth, and 60-cm relative distance) and deployed at a speed of 0.1 m s^{-1}, at 7.5 m from the main structure of the AAOT. The rigidity and stability of the rig is maintained through two taut wires anchored between the tower and a weight on the sea bottom, which prevent the movement of the rig out of the vertical plane of the wires. The wire stabilization and the relatively low deployment speed ensure a good optical characterization of the subsurface water layer. In addition, unlike winched or crane systems operated from ships, the immovability of the AAOT does not produce supplementary perturbations adding to wave effects.

WiSPER provides profiles of $L_u(z, \lambda)$, $E_u(z, \lambda)$, and $E_d(z, \lambda)$ with a 6-Hz acquisition rate in seven spectral bands 10 nm wide, centered at 412, 443, 490, 510, 555, 665, and 683 nm. The system is equipped with Satlantic (Halifax, Nova Scotia, Canada) radiometers: an OCR-200 for $L_u(z, \lambda)$ with approximately 20° full aperture field of view, two OCI-200 for $E_d(z, \lambda)$ and $E_u(z, \lambda)$ with independent collectors of ~1-cm diameter for each channel, and an additional OCI-200 installed on the uppermost level of the tower for the above-water downward irradiance $E_d(0^+, \lambda)$. The latter data are required to correct the in-water measurements for changes in the illumination conditions during casts. A schematic of the AAOT and of the WiSPER system is shown in Fig. 1.

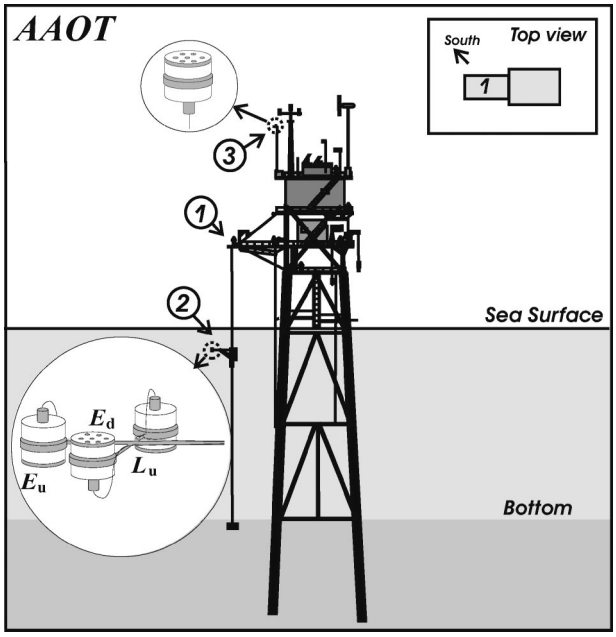

FIG. 1. Schematic of the AAOT: 1) the WiSPER deployment platform, 2) the WiSPER system [the inset shows the in-water radiometers used for $L_u(z, \lambda)$, $E_u(z, \lambda)$, and $E_d(z, \lambda)$ measurements], and 3) the reference radiometer for $E_d(0^+, \lambda)$ measurements.

b. Data processing

Processing of WiSPER data was carried out using an optical processor system developed at the Joint Research Centre (JRC) for the analysis of the CoASTS data (D'Alimonte et al. 2001). The applied processing steps are summarized here for completeness.

In-water radiometric quantities (in physical units) were normalized with respect to $E_d(0^+, \lambda, t)$, with t explicitly expressing the dependence on time, according to

$$\Re(z, \lambda, t_0) = \Re(z, \lambda, t)\frac{E_d(0^+, \lambda, t_0)}{E_d(0^+, \lambda, t)}, \qquad (1)$$

where $\Re(z, \lambda, t_0)$ identifies the radiometric quantities [i.e., $L_u(z, \lambda, t)$, $E_u(z, \lambda, t)$, and $E_d(z, \lambda, t)$] as they were taken at all absolute depths z at the same time t_0, $E_d(0^+, \lambda, t)$ is the above-water irradiance taken at the same time t of the in-water $\Re(z, \lambda, t)$ data, while $E_d(0^+, \lambda, t_0)$ is the above-water irradiance at time t_0 (where t_0

TABLE 1. Typical uncertainty budget of WiSPER data.

	L_u			E_u			E_d		
Major uncertainties	443	555	665	443	555	665	443	555	665
Absolute calibration (%)	2.8	2.8	2.8	2.2	2.2	2.2	2.2	2.2	2.2
Uncertainty in corrections (%)	1.3	1.4	2.3	1.2	1.5	1.4	0.8	0.3	0.2
Environmental variability (%)	2.1	2.2	3.2	2.0	2.1	2.9	3.0	3.3	4.2
Quadrature sum (%)	3.7	3.8	4.8	3.2	3.4	3.9	3.8	4.0	4.8

was chosen as to coincide with the start of the cast). For simplicity the variable t is hereafter omitted.

The appropriateness of the extrapolation interval, satisfying the requirement of linear decay of $\ln\Re(z, \lambda)$, was evaluated on a cast-by-cast basis by successive trials choosing a specific optical quantity (i.e., L_u or E_d) and wavelength. The use of E_d at $\lambda = 665$ nm was considered the most appropriate. The existence of large differences between subsurface $E_d(0^-, \lambda)$ and above-water $E_d(0^+, \lambda)$ values highlighted cases for which the selection of the extrapolation interval was not appropriate. The use of a red channel, where seawater is characterized by a high absorption and the data show a fast drop to noise levels as a function of depth, helped in excluding irrelevant data from the extrapolation interval.

Self-shading, tower shading, and bottom effects were removed assuming all perturbations independent from each other (Zibordi et al. 2002).

The subsurface primary quantities $\Re(0^-, \lambda)$ [i.e., $L_u(0^-, \lambda)$, $E_d(0^-, \lambda)$, and $E_u(0^-, \lambda)$] are the exponents of the intercept given by the least squares linear regressions of $\ln\Re(z, \lambda)$ versus z, within the extrapolation interval identified by $z_0 < z < z_1$. Generally, for CoASTS profiles, $0.3 < z_0 < 1.0$ m and $2.5 < z_1 < 4.5$ m. The negative values of the slopes of the regression fits are the so-called diffuse attenuation coefficients $K_{\Re}(\lambda)$ [i.e., $K_l(\lambda)$, $K_d(\lambda)$, and $K_u(\lambda)$] for the extrapolation interval.

In addition to the primary quantities $\Re(z, \lambda)$ and $K_{\Re}(\lambda)$, derived quantities like the subsurface Q factor at nadir $Q_n(\lambda)$, the subsurface irradiance reflectance $R(\lambda)$, and the normalized water-leaving radiance, $L_{\text{WN}}(\lambda)$, were computed according to

$$Q_n(\lambda) = \frac{E_u(0^-, \lambda)}{L_u(0^-, \lambda)}, \tag{2}$$

$$R(\lambda) = \frac{E_u(0^-, \lambda)}{E_d(0^-, \lambda)}, \quad \text{and} \tag{3}$$

$$L_{\text{WN}}(\lambda) = \overline{F}_0(\lambda)\frac{0.54L_u(0^-, \lambda)}{E_d(0^+, \lambda)}, \tag{4}$$

where $\overline{F}_0(\lambda)$ is the mean extraterrestrial solar irradiance and 0.54 accounts for the in-water reflectance of sea surface for upwelling radiance.

The normalized water-leaving radiance $L_{\text{WN}}(\lambda)$ was also computed using above-water downward irradiance values derived from the $E_d(0^-, \lambda)$ values extrapolated above the surface, here defined as $\breve{E}_d(0^+, \lambda)$ and given by

$$\breve{E}_d(0^+, \lambda) = \frac{E_d(0^-, \lambda) - 0.49E_u(0^-, \lambda)}{1 - \rho_s(\lambda)}, \tag{5}$$

where the coefficient 0.49 (Mobley 1994) is an estimate of the subsurface reflectance for upward irradiance and $\rho_s(\lambda)$ is the sea surface reflectance for downward irradiance given by

$$\rho_s(\lambda) = \frac{\rho_0(\lambda) + 0.066r(\lambda)}{1 + r(\lambda)}, \tag{6}$$

with $\rho_0(\lambda)$ the Fresnel reflectance of the sea surface at the sun zenith angle θ_0, $r(\lambda)$ the diffuse over direct irradiance ratio, and 0.066 the sea surface albedo under diffuse illumination. Under clear-sky conditions, characterized by a low $r(\lambda)$, $\rho_s(\lambda) \rightarrow \rho_0(\lambda)$.

The normalized water-leaving radiances computed using $\breve{E}_d(0^+, \lambda)$ are hereafter identified as $\breve{L}_{\text{WN}}(\lambda)$.

c. Uncertainty budget of WiSPER data

The major uncertainties affecting the absolute WiSPER measurements can be summarized by (a) radiometric calibration uncertainties resulting from the uncertainties in the in-air absolute calibration and immersion coefficient, and from the sensitivity change between successive calibrations; (b) uncertainties in the correction factors applied for removing self-shading, tower shading, and bottom effects; and (c) environmental variability resulting from the combination of wave-induced perturbations with seawater variability and illumination changes. Typical values for the three highlighted classes of uncertainties are presented in Table 1 for $L_u(z, \lambda)$, $E_u(z, \lambda)$, and $E_d(z, \lambda)$ at the center wavelengths 443, 555, and 665 nm, chosen as representative of the visible spectrum.

The uncertainties for the absolute radiometric calibration values of $L_u(z, \lambda)$ were computed as the quadrature sum of 2.1%, the typical uncertainty in the in-air absolute calibration (Zibordi et al. 2002); 1%, the assumed maximum uncertainty in the value of the immersion coefficient; and 1.5%, the assumed instrument sensitivity change between calibrations. The uncertainties for the absolute radiometric calibration values of $E_u(z, \lambda)$ and $E_d(z, \lambda)$ were computed as the quadrature

sum of 1.5%, the typical uncertainty in the in-air calibration (Zibordi et al. 2002); 0.5% the uncertainty in the value of the immersion coefficient for individually characterized collectors (Zibordi et al. 2004); and 1.5%, the assumed instrument sensitivity change between calibrations.

The uncertainty values of the applied corrections for self-shading (Zibordi and Ferrari 1995; Mueller and Austin 1995), tower shading (Doyle and Zibordi 2002; Doyle et al. 2003), and bottom effects (Zibordi et al. 2002) were determined assuming an arbitrary uncertainty of 25% in each single correction factor applied to the data used in this study.

The uncertainty values related to the environmental variability were estimated here from differences in $L_u(0^-, \lambda)$, $E_u(0^-, \lambda)$, and $E_d(0^-, \lambda)$ determined from 36 pairs of consecutive WiSPER profiles. The differences between the radiometric values determined from these consecutive profiles collected with a 10-min delay from each other were attributed to variability in the seawater and illuminations conditions, and to wave-induced perturbations.

The quadrature sum of the three major types of uncertainties for L_u shows values close to the 5% target established for the absolute radiometric accuracy of current ocean color sensors (Hooker and Esaias 1993). Considering that the uncertainty produced by the environmental variability was determined here with the high depth resolution WiSPER measurements likely minimizing the focusing and defocusing perturbations in the extrapolated subsurface quantities, it is of relevance to separately determine the wave-induced perturbations as a function of the depth resolution of the profile data to evaluate their impact on a typical uncertainty budget.

4. Data analysis

The specific objective of this work was to determine the depth resolution requirements for optical profiling in coastal waters, which restrict below a defined threshold the uncertainties in subsurface primary and derived quantities in the presence of wave focusing and defocusing. This is in keeping with the need to produce accurate in situ measurements comparable to satellite observations and including averaged wave effects. In the case of remote sensing data the wave effects are spatially averaged over the area determined by the instantaneous field of view of the space sensor. In the case of in situ profile data the averaging occurs over time as a function of the depth and optics features.

Sample WiSPER $L_u(z, \lambda)$ and $E_d(z, \lambda)$ profiles are presented in Fig. 2 for different measurement conditions characterized by a wave height of ~10 cm with $K_d(490) = 0.20\ m^{-1}$ determined in the 0.3–2.5-m extrapolation interval (Figs. 2a,b), and by a wave height of ~40 cm with $K_d(490) = 0.09\ m^{-1}$ determined in the 0.3–4.0-m extrapolation interval (Figs. 2c,d). The semilogarithmic plot of the $L_u(z, \lambda)$ data in Fig. 2a does not show relevant surface perturbation effects, but highlights the presence of a nonlinear change with depth. This occurs between 3- and 6-m depth and was produced by a gradient in the vertical distribution of optically significant seawater components as confirmed by simultaneous profiles of inherent optical properties. The observed changes in the linearity with depth of the log-transformed $L_u(z, \lambda)$ data restrict the extrapolation interval to the first 3 m below the surface. The $E_d(z, \lambda)$ data in Fig. 2b exhibit wave focusing and defocusing effects, highlighted by signal fluctuations decreasing with depth. The high signal variations observed in the first tens of centimeters just below the surface suggest an exclusion of related data from the extrapolation interval. The semilogarithmic plot of the $L_u(z, \lambda)$ data in Fig. 2c does not display any departure from linearity with depth. However both the $L_u(z, \lambda)$ and $E_d(z, \lambda)$ data in Figs. 2c and 2d show larger fluctuations extending at higher depths with respect to the profiles displayed in panels Figs. 2a and 2b. These examples, produced with a given class of commercial instruments, suggest a dependence of the accuracy in subsurface quantities on depth resolution of profile data.

An uncertainty analysis was carried out by comparing the subsurface optical values computed with full-resolution reference profiles and with reduced resolution profiles, keeping the same extrapolation intervals. Reduced depth resolution profiles were obtained by decreasing the number of data in the full-resolution WiSPER downcast profiles characterized by ~64 measurements per meter corresponding to a depth resolution Δz_{N_0} higher than ~1.6 cm. Specifically, profiles with $N = 32$, 16, 8, 4, and 2 measurements per meter corresponding to depth resolutions Δz_N of 3.125, 6.25, 12.5, 25, and 50 cm, were produced by keeping data every n increment steps in the full-resolution profiles (i.e., $n = 2$, 4, 8, 16, and 32, respectively). The comparisons among subsurface quantities produced with these different depth resolution profiles are then based on the adoption of the same data acquisition period equal to 1/6 s. This is expected to reflect the actual measurement conditions for decreased depth resolution profiles on the following assumptions: 1) random focusing and defocusing effects and 2) comparability, over a large number of profiles, between wave perturbations affecting the single measurements related to depth intervals $z \pm 1/2\Delta z_{N_0}$ and those related to the larger depth intervals $z \pm 1/2\Delta z_N$.

The implicit application of the same calibration coefficients and correction factors to both full- and reduced resolution profiles ensured the independence of the results from any uncertainty related to the applied calibration and corrections. The normalization of profile data with respect to the above-water downward irradiance, by choosing the start of the cast as the reference time in Eq. (1), made the analysis independent of any slight changes in the illumination conditions during the data collection. The homogeneity of the water column in the extrapolation interval, assessed during the pro-

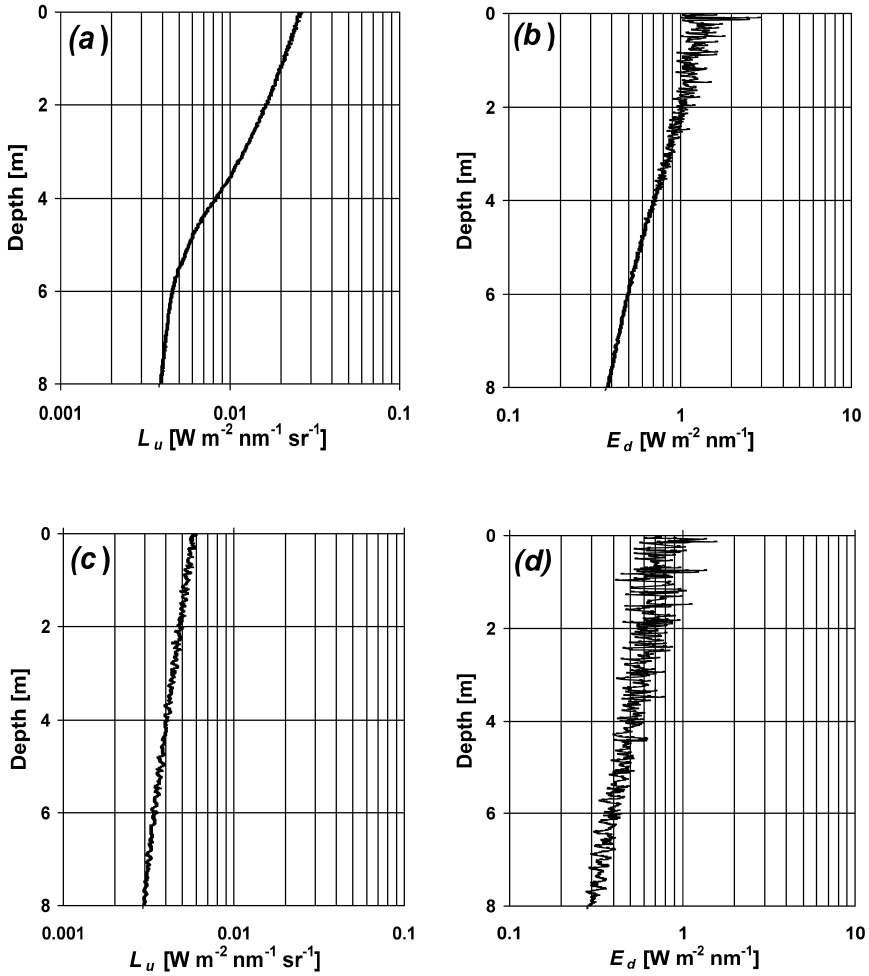

FIG. 2. WiSPER $L_u(z, \lambda)$ and $E_d(z, \lambda)$ profiles at $\lambda = 555$ nm taken on (a), (b) 8 Jul 2002 with ~10-cm-average waves height and a diffuse attenuation coefficient $K_d(490) = 0.20$ m^{-1} at 490 nm and on (c), (d) 17 Sep 2002 with ~40-cm wave height and $K_d(490) = 0.09$ m^{-1}.

cessing of full-resolution profiles, guaranteed that gradients in the vertical distribution of the seawater components did not affect the analysis.

In conclusion, the proposed scheme relied on the comparison of subsurface quantities determined from profile data differing by depth resolutions, but characterized by identical (i) acquisition rate, (ii) optical characteristics of radiometers, (iii) extrapolation interval, and (iv) illumination changes and seawater characteristics. These conditions ruling the comparisons of subsurface values from reduced and full-resolution profile made the uncertainty analysis depend on wave-induced perturbations only.

a. Data and methods

The following data analysis is presented through the most relevant primary optical quantities, that is, those directly computed from the optical profiles, and specifically the subsurface values $L_u(0^-, \lambda)$, $E_u(0^-, \lambda)$, and $E_d(0^-, \lambda)$, and the diffuse attenuation coefficient $K_d(\lambda)$ relative to the extrapolation interval.

The dataset used in the study includes 244 profiles collected in the period January 1999–February 2001 on very different environmental conditions with a 38% occurrence of Case-2 waters, and satisfying the following criteria: (i) cloud cover lower than 2/4, (ii) clear sun conditions, (i.e., the sun not covered by clouds), and (iii) wind speed lower than 10 m s^{-1} to minimize perturbations due to wave breaking. The average value of quantities identifying the measurement conditions and the extrapolation intervals for the 244 profiles are listed in Table 2. Specific quantities are the absorption of colored dissolved organic matter, a_y at 412 nm; the total chlorophyll-*a* resulting from the sum of chlorophyll-*a*, *Chla*, and chlorophyllide-*a*, *Chlide*; and the total suspended matter, TSM. Additional quantities are the wind speed, W_s; the sun zenith, θ_0; the ratio of diffuse to

TABLE 2. Range, average, and standard deviation of quantities characterizing the data set used for the present study.

Quantity	Range	Avg ± std dev
a_y (412) (m^{-1})	0.02–0.26	0.121 ± 0.044
Chla + Chlide ($\mu g\ L^{-1}$)	0.21–4.74	1.24 ± 0.95
TSM (mg L^{-1})	0.2–3.7	1.05 ± 0.63
W_S (m s^{-1})	0.4–9.7	3.3 ± 2.0
θ (°)	22.1–70.8	43.5 ± 15.4
r(412) (−)	0.16–1.58	0.72 ± 0.30
Extrapolation interval (m)	0.3–0.6, 2.5–5.0	0.41 ± 0.04, 3.56 ± 0.47

direct above-water downward irradiance, r, at 412 nm; and the limits of the extrapolation intervals used for the computation of the values for subsurface quantities.

The comparison of quantities obtained from full- and reduced resolution profiles characterized by the selected number of measurements per meter are presented and summarized through average percent differences, ψ; average absolute percent differences, $|\psi|$; and determination coefficients, r^2, from least squares regressions of M profiles and L channels. While ψ highlights the existence of a bias between the compared quantities, $|\psi|$ preserves the variance and quantifies the average uncertainty.

The values of ψ were computed through

$$\psi = \frac{1}{L}\frac{1}{M}\sum_{j=1}^{L}\sum_{m=1}^{M}\psi_{j,m}, \tag{7}$$

where j indicates the channel index, m is the profile index, and $\psi_{j,m}$ is given by

$$\psi_{j,m} = 100\frac{\Re^{N}(j)_m - \Re^{N_0}(j)_m}{\Re^{N_0}(j)_m}, \tag{8}$$

where the superscript N indicates the subsurface quantities computed from reduced resolution profiles (those defined by $N = 2$–32 samples per meter), and the superscript N_0 indicates the reference quantities computed from full-resolution profiles (those defined by $N = 64$ samples per meter). The absolute values of $\psi_{j,m}$, $|\psi_{j,m}|$ were used to compute the average absolute percentage differences $|\psi|$ according to

$$|\psi| = \frac{1}{L}\frac{1}{M}\sum_{j=1}^{L}\sum_{m=1}^{M}|\psi_{j,m}|. \tag{9}$$

b. Results

The scatterplots in Fig. 3 display the primary quantities computed with a decreased depth resolution defined by $N = 8$ samples per meter versus the same quantities computed with full-resolution profiles defined by $N = 64$ samples per meter.

The scatterplots highlight the higher uncertainties for $E_d(0^-, \lambda)$ and $K_d(\lambda)$ values (Figs. 3c and 3d) than for $L_u(0^-, \lambda)$ and $E_u(0^-, \lambda)$ values (Figs. 3a and 3b). The different uncertainties are mostly explained by the direct transmission of flashes for $E_d(z, \lambda)$ and differently by their transmission through backscattering for $L_u(z, \lambda)$ and $E_u(z, \lambda)$.

The occurrence of negative $K_d(\lambda)$ values among data computed from the reduced depth resolution profiles (see Fig. 3d) is a clear indication of the appreciable perturbations affecting the computation of subsurface values.

The spectral uncertainty analysis is presented in Table 3 as a function of N—at center wavelengths $\lambda = 412$, 443, 490, 510, 555, 665, and 683 nm—for each primary quantity. All the quantities show an expected increase in $|\psi|$ for a decrease in N and confirm larger uncertainties for $E_d(0^-, \lambda)$ and $K_d(\lambda)$, with respect to $L_u(0^-, \lambda)$ and $E_u(0^-, \lambda)$. The two last quantities exhibit similar results for all of the considered cases, with r^2 (not shown) always equal to 1.00. Their spectral uncertainties show almost constant $|\psi|$ values from 412 to 555 nm. They exhibit values increasing from 0.1% to 1.8% for $L_u(0^-, \lambda)$ and from 0.1% to 1.4% for $E_u(0^-, \lambda)$, as N decreases from 32 to 2. More pronounced $|\psi|$ values are observed at 665 and 683 nm, increasing from 0.3% to 4.0% for $L_u(0^-, \lambda)$ and from 0.2% to 2.6% for $E_u(0^-, \lambda)$, with decreasing N. These slightly smaller spectral uncertainties in the blue-green, when compared to the red, can be explained by a higher scattering of seawater in the blue-green increasing the diffuseness of the light field and consequently decreasing the effects of wave-induced perturbations.

Unlike from the blue-green channels, the red channels at 665 and 683 nm show a general increase in ψ as N decreases, exhibiting values reaching 0.9% with $N = 2$ for both $L_u(0^-, \lambda)$ and $E_u(0^-, \lambda)$. This spectral dependence is again explained by a lower diffuseness of the light field in the red than at shorter wavelengths. The positive bias can be explained by the high weight of the measurements affected by wave focusing in the extrapolation process through an exponential function. This weight positively biases the near-surface values when the measurement distribution does not comprehensively describe the wave perturbations, as likely occurs with decreasing depth resolution.

Here $E_d(0^-, \lambda)$ shows values of $|\psi|$ increasing from 0.9% at 412 nm to 1.4% at 683 nm with $N = 32$, and from 8.5% at 412 nm to 14.5% at 683 nm with $N = 2$. The regular increase with wavelength is again explained

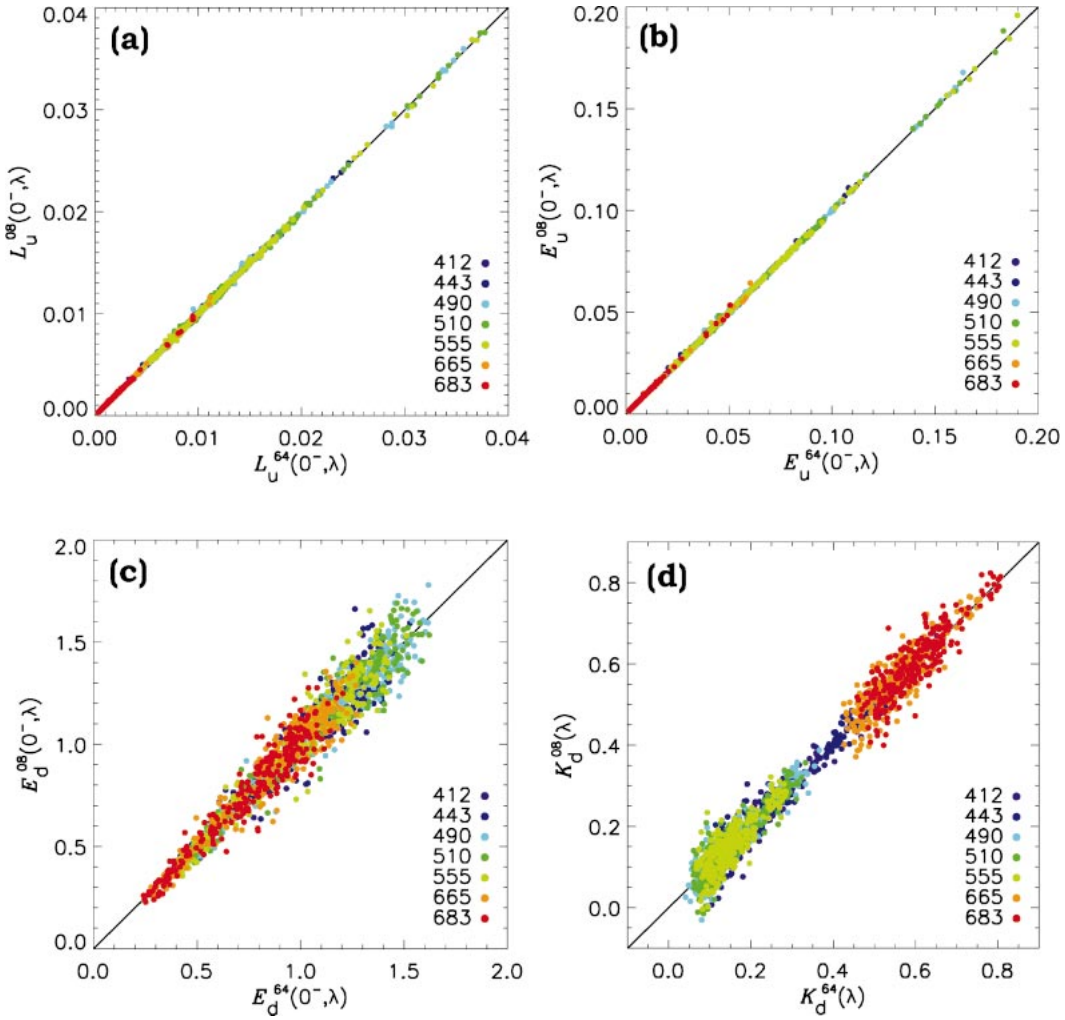

FIG. 3. Scatterplot of primary optical quantities (a) $L_u(0^-, \lambda)$, (b) $E_u(0^-, \lambda)$, (c) $E_d(0^-, \lambda)$, and (d) $K_d(\lambda)$ obtained with decreased resolution profile data (i.e., $N = 8$) vs the reference values obtained from full resolution profile data (i.e., $N = 64$). Radiances $L_u(0^-, \lambda)$ are in units of W m^{-2} nm^{-1} sr^{-1}, irradiances $E_u(0^-, \lambda)$ and $E_d(0^-, \lambda)$ are units of W m^{-2} nm^{-1}, and $K_d(\lambda)$ in units of m^{-1}.

by the scattering properties of seawater, whose decrease produces an increase in the wave focusing and defocusing effects. The ψ values for $E_d(0^-, \lambda)$ appreciably increase as N decreases and exhibit a general increase with wavelength (excluding data at 555 nm) from 0.9% at 412 nm to 3.7% at 683 nm. The corresponding analysis of r^2 (not shown) exhibits values decreasing as N decreases and as wavelength increases. For $N = 2$, the r^2 values decrease from 0.91 at 412 nm to 0.82 at 683 nm. This is also explained by a decrease in seawater scattering, leading to more pronounced wave effects and thus increasing the dispersion of data.

Among all analyzed quantities $K_d(\lambda)$ shows the highest uncertainties. The spectral $|\psi|$ values increase from 1.5% at 412 nm to 3.5% at 555 nm with $N = 32$ and from 15.3% at 412 nm to 47.8% at 555 nm with $N = 2$. The red channels show much lower $|\psi|$ values, when compared to the blue-green channels, with an increase from 1.1% with $N = 32$ to 11.1% with $N = 2$. This can be explained by the fact that, assuming the same perturbations affecting all wavelengths in the 412–683-nm spectral range, $K_d(\lambda)$ is subject to the smallest percent variations in the red where its value is the highest. The spectral dependence of the ψ values generally reflects that observed for $|\psi|$. Specifically, with $N = 2$ the analysis of $K_d(\lambda)$ data shows values of ψ increasing from 3% at 412 nm up to 15% at 490 nm, and dropping to average values of 3% in the red at 665 and 683 nm. The spectral analysis of r^2 for $N = 2$ (not shown) exhibits decreasing values from 0.9 at 412 nm to 0.6 at 555 nm, and average values of 0.7 in the red.

The appreciable increase of the spectral ψ values observed for $K_d(\lambda)$ and $E_d(0^-, \lambda)$ as N decreases, as for $L_u(0^-, \lambda)$ and $E_u(0^-, \lambda)$, is explained by the high

TABLE 3. Spectral uncertainty values (%) for different depth resolutions.

		412		443		490		510		555		665		683	
	N	$\lvert\psi\rvert$	ψ	$\lvert\psi\rvert$	ψ	$\lvert\psi\rvert$	ψ	$\lvert\psi\rvert$	ψ	$\lvert\psi\rvert$	ψ	$\lvert\psi\rvert$	ψ	$\lvert\psi\rvert$	ψ
L_u	32	0.11	0.01	0.11	0.01	0.12	0.01	0.12	0.01	0.14	0.02	0.28	0.05	0.28	0.00
	16	0.36	0.01	0.34	0.00	0.34	−0.02	0.36	−0.01	0.41	−0.01	0.97	0.04	1.01	0.11
	8	0.76	−0.01	0.71	−0.07	0.71	−0.03	0.71	−0.13	0.74	−0.13	1.78	0.01	1.74	0.14
	4	1.21	0.00	1.14	−0.03	1.21	−0.02	1.19	−0.10	1.27	−0.10	2.75	0.44	2.85	0.83
	2	1.72	−0.01	1.73	0.11	1.68	0.08	1.74	−0.07	1.81	0.10	3.95	0.73	4.09	0.85
E_u	32	0.08	0.01	0.09	0.01	0.10	−0.01	0.10	0.01	0.10	0.01	0.18	0.01	0.20	0.00
	16	0.21	−0.02	0.20	−0.01	0.26	−0.04	0.28	−0.02	0.31	−0.04	0.45	0.11	0.51	0.15
	8	0.45	−0.04	0.44	−0.06	0.49	−0.03	0.50	−0.10	0.51	−0.06	1.02	0.19	1.10	0.31
	4	0.96	−0.04	0.92	−0.03	1.00	−0.15	0.97	−0.18	1.04	−0.18	1.74	0.30	1.85	0.67
	2	1.29	0.02	1.22	−0.10	1.28	−0.05	1.35	−0.14	1.36	−0.04	2.58	0.64	2.67	0.93
E_d	32	0.85	0.03	0.85	0.07	0.99	0.08	1.04	−0.06	1.14	0.00	1.42	0.01	1.35	−0.01
	16	2.15	−0.09	2.49	−0.03	2.82	−0.01	3.21	0.03	3.22	0.30	3.55	0.31	3.86	0.16
	8	3.97	0.69	4.49	0.45	4.75	0.53	5.27	0.90	5.72	0.73	6.31	1.33	6.39	1.21
	4	5.80	0.00	6.30	0.22	7.29	0.83	7.69	0.50	9.02	1.11	9.97	1.35	9.39	1.26
	2	8.49	0.96	9.30	1.27	10.18	2.24	11.44	2.46	12.53	1.56	13.43	2.54	14.52	3.74
K_d	32	1.50	0.21	1.96	0.36	3.37	0.51	3.49	0.32	3.52	−0.15	1.13	−0.01	1.00	0.03
	16	3.91	−0.08	5.48	0.13	10.63	0.49	10.88	1.10	10.35	1.15	2.68	0.06	2.65	0.10
	8	8.53	1.66	12.08	2.15	17.80	2.48	19.10	3.76	18.70	4.00	5.11	0.71	5.02	0.87
	4	10.51	0.44	16.03	2.12	27.98	7.81	28.77	10.25	31.43	7.87	7.60	0.73	6.84	0.73
	2	15.30	3.03	25.44	9.11	45.71	15.11	46.38	12.32	47.75	10.23	11.02	3.01	11.12	3.04

weight of the measurements affected by wave focusing in the extrapolation process through an exponential function.

The large increase observed in the spectral values of ψ for $E_d(0^-, \lambda)$ and $K_d(\lambda)$ as N decreases does not similarly appear for $L_u(0^-, \lambda)$ and $E_u(0^-, \lambda)$. This is again explained by the higher diffuseness of the upward light field with respect to the downward one.

The nonappreciable differences in both the $|\psi|$ and ψ values at 665 and 683 nm suggest a nonrelevant contribution from fluorescence in the reduction of wave-induced perturbations at 683 nm. In addition, due to the near-surface depths considered in the study, the Raman scattering is also assumed to not produce any appreciable effect on the uncertainty analysis.

TABLE 4. Uncertainty values (%) determined for spectral-ratio quantities.

		443/555		490/555		510/555	
	N	$\lvert\psi\rvert$	ψ	$\lvert\psi\rvert$	ψ	$\lvert\psi\rvert$	ψ
L_u	32	0.09	0.00	0.08	0.01	0.05	0.01
	8	0.44	0.07	0.37	0.08	0.30	0.04
	2	0.98	0.16	0.72	0.05	0.51	0.00
E_d	32	0.88	−0.06	0.86	−0.09	0.59	−0.05
	8	3.87	−0.13	3.46	−0.11	2.54	−0.03
	2	8.43	0.35	7.53	0.97	4.60	0.10
L_{WN}	32	0.09	0.00	0.07	0.00	0.05	0.01
	8	0.43	0.07	0.38	0.07	0.30	0.04
	2	0.98	0.17	0.72	0.06	0.51	0.01
$\check{L}_{WN}$	32	0.95	0.06	0.96	0.12	0.63	0.08
	8	4.16	0.63	3.79	0.50	2.77	0.36
	2	9.06	0.96	8.07	0.28	4.94	0.29

Spectral ratios are of relevance in the development of biooptical algorithms (O'Reilly et al. 1998). Uncertainties in their computed values due to wave perturbations are presented in Table 4 for $L_u(0^-, \lambda_1)/L_u(0^-, \lambda_2)$, $E_d(0^-, \lambda_1)/E_d(0^-, \lambda_2)$, and for the derived quantities $L_{WN}(\lambda_1)/L_{WN}(\lambda_2)$ and $\check{L}_{WN}(\lambda_1)/\check{L}_{WN}(\lambda_2)$ at center wavelengths $\lambda_1 = 443$, 490, and 510 nm, and $\lambda_2 = 555$ nm. The last two derived quantities are those having direct application in biooptical modeling.

The comparison of data in Tables 3 and 4 shows a general reduction in the $E_d(0^-, \lambda_1)/E_d(0^-, \lambda_2)$ uncertainties with respect to those of the individual spectral quantities $E_d(0^-, \lambda_1)$ and $E_d(0^-, \lambda_2)$. A reduction, though less pronounced, is also observed in the $L_u(0^-, \lambda_1)/L_u(0^-, \lambda_2)$ uncertainties with respect to those determined for $L_u(0^-, \lambda_1)$ and $L_u(0^-, \lambda_2)$. These reductions suggest the existence of a correlation between the uncertainties at the different wavelengths. The uncertainties presented in Table 4 show a decrease as λ_1 increases. This result can be explained by the design of the radiometers utilized for the data collection and more specifically by the decreasing distance between the λ_1 and λ_2 optics as λ_1 increases (e.g., the 510-nm optics is closer to the 555-nm one than is the 443-nm one). In fact, the optics of the different channels for both the radiance and irradiance radiometers used in this study are independent and distributed within a circle of ~4-cm diameter. Because of this, random perturbations produced by wave focusing affect the signal detected in the various channels differently. It is then reasonable to as-

sume that the wave-induced perturbations tend to become more comparable at different wavelengths when their optics are closer. This further confirms the dependence of wave-induced perturbations on the geometry of optics, and implicitly on the field of view of radiance sensors and the diameter of irradiance collectors.

The comparison of $|\psi|$ for $L_{WN}(0^-, \lambda_1)/L_{WN}(0^-, \lambda_2)$ and $L_u(0^-, \lambda_1)/L_u(0^-, \lambda_2)$ shows almost identical values because of the independence of $E_d(0^+, \lambda_2)/E_d(0^+, \lambda_1)$ from wave perturbations. On the other hand, the $|\psi|$ values for $\check{L}_{WN}(0^-, \lambda_1)/\check{L}_{WN}(0^-, \lambda_2)$ appear close to the sum of those for the quantities used in their computation, that is, $L_u(0^-, \lambda_1)/L_u(0^-, \lambda_2)$ and $\check{E}_d(0^-, \lambda_1)/\check{E}_d(0^-, \lambda_2)$. An extended analysis of uncertainties in the derived quantities, and specifically on $L_{WN}(0^-, \lambda)$ and $\check{L}_{WN}(0^-, \lambda)$, is presented in the discussion section.

c. Accuracy of computed uncertainties

The data analysis was made on the assumption that the intrinsic uncertainties induced by wave perturbations in the computation of subsurface quantities from full-resolution profiles did not affect the accuracy of the $|\psi|$ and ψ data. A sensitivity analysis carried out using as reference values the primary quantities computed with the $N = 32$ reduced resolution profiles (where the ψ values are generally not appreciable) produced the same uncertainties for $N = 16$, 8, 4, and 2 as those obtained using as reference values the primary quantities computed with the $N = 64$ full-resolution profiles.

This is explained by the percent differences between the $\Re^N(j)_m$ and $\Re^{N_0}(j)_m$ values [see Eq. (8)]. In fact, under the condition of the normal distribution of uncertainties due to random focusing and defocusing effects, where the wave perturbations affecting $\Re^N(j)_m$ and $\Re^{N_0}(j)_m$ are both equally dependent on the number of samples per meter, it is reasonable to assume that the averaging of the percent differences between the $\Re^N(j)_m$ and $\Re^{N_0}(j)_m$ values leads to the determination of very close statistical uncertainties $|\psi|$ and biases ψ for subsurface quantities computed with the same number of measurements per meter, N, regardless of the depth resolution characterizing the reference profiles.

This finding suggests that the computed $|\psi|$ and ψ values are not significantly dependent on the wave-induced perturbations affecting the reference primary quantities and, consequently, they are suitable for estimating the accuracy requirements for optical profiling in coastal waters.

5. Discussion

Different analyses of the dataset were made to address the dependence of wave perturbations on environmental quantities like the sea state, S_s, applied as a wave height index; the diffuse attenuation coefficient at 490 nm, $K_d(490)$, applied as a seawater optical index for the extrapolation layer; the sun zenith, θ_0, and the diffuse to direct downward irradiance ratio at 412 nm, $r(412)$, both applied as illumination indices. The results from the analyses exhibited an appreciable dependence of the uncertainties on the first two indices and only their slight increase as both θ_0 and r decrease for the specific measurement conditions characterizing the dataset reported in Table 2.

This section mostly discusses the dependence of wave effects on changes in the sea state and diffuse attenuation coefficient, and additionally presents the minimum depth resolution requirements constraining wave-induced uncertainties below 1%, 2%, and 5% in the determination of subsurface optical quantities.

a. Uncertainties as a function of sea state and of $K_d(490)$

The dependence of uncertainties on sea state was analyzed by partitioning the dataset according to $S_s = 1$, 2, and 3 [here corresponding to wave heights of 0–0.1, 0.1–0.5, and 0.5–1.25 m, respectively, according to the WMO (1983) scale]. The dependence on the diffuse attenuation coefficient was analyzed using $K_d(490)$ computed from full-resolution profiles, and partitioning the dataset into two classes defined by $K_d(490) < 0.14$ m^{-1} and $K_d(490) \geq 0.14$ m^{-1} (where the value 0.14 m^{-1} is close to the median computed for the set of full-resolution profiles). In Table 5 the data analysis is presented through the spectral average of uncertainties at 443, 555, and 665 nm with $N = 32$, 8, and 2, for the primary and for a few derived quantities. The latter include $R(\lambda)$, $Q_n(\lambda)$, $L_{WN}(\lambda)$, and $\check{L}_{WN}(\lambda)$. The remote sensing reflectance, that is, $R_{rs}(\lambda)$, a derived quantity widely used in remote sensing applications, was not included in the sensitivity analysis because it only differs from $L_{WN}(\lambda)$ by a spectral constant (Mueller and Austin 1995). Thus any conclusions reached for $L_{WN}(\lambda)$ equally apply to $R_{rs}(\lambda)$.

The analysis of the spectral average $|\psi|$ values as a function of sea state shows an increase for all primary and derived quantities [with the exception of $E_u(0^-, \lambda)$] from $S_s = 1$ to $S_s = 2$, and a general decrease from $S_s = 2$ to $S_s = 3$. Within the primary quantities, the largest effects on sea state change in the S_1–S_3 range are observed for $K_d(\lambda)$ with $N = 2$. Specifically, from $S_s = 1$ to $S_s = 2$ the uncertainty increases from 26.1% to 31.4%, and then drops to 14.1% at $S_s = 3$. The corresponding uncertainty in $E_d(0^-, \lambda)$ increases from 8.9% at $S_s = 1$ to 13.6% at $S_s = 2$, and then drops to 9.3% at $S_s = 3$. The observed decrease can be attributed to enhanced superimposition of waves (characterized by a different height and amplitude) increasing the in-water diffuse light field. This adds to the wave breaking and to the appearance of foam and whitecaps at the surface, which also contribute to a general increase of the in-water light diffuseness and to a consequent reduction of wave-induced effects. The explanation may fail in cases of large swell following a decrease in wind speed.

TABLE 5. Spectral average uncertainties (%) as function of sea state, S_s, and diffuse attenuation coefficient, $K_d(490)$; M indicates the number of profiles used for each analysis.

		All (M = 244)		S_s = 1 (M = 62)		S_s = 2 (M = 141)		S_s = 3 (M = 41)		$K_d < 0.14$ (M = 123)		$K_d \geq 0.14$ (M = 121)	
	N	$\lvert\psi\rvert$	ψ	$\lvert\psi\rvert$	ψ	$\lvert\psi\rvert$	ψ	$\lvert\psi\rvert$	ψ	$\lvert\psi\rvert$	ψ	$\lvert\psi\rvert$	ψ
L_u	32	0.17	0.02	0.14	0.02	0.18	0.03	0.18	0.02	0.21	0.03	0.14	0.01
	8	1.00	−0.11	0.84	−0.09	1.07	−0.16	1.07	0.10	1.22	−0.09	0.82	−0.11
	2	2.33	0.13	1.71	−0.09	2.58	0.22	2.48	0.51	2.55	0.03	2.23	0.20
E_u	32	0.13	0.01	0.11	0.01	0.12	0.00	0.15	0.01	0.14	0.01	0.10	0.00
	8	0.63	0.00	0.52	0.01	0.65	−0.01	0.64	0.01	0.67	0.09	0.59	−0.08
	2	1.65	0.15	1.24	−0.03	1.68	0.19	2.34	0.29	1.60	0.02	1.72	0.30
E_d	32	1.16	0.05	1.21	−0.17	1.27	0.20	0.86	−0.09	1.41	0.06	0.97	0.01
	8	5.51	0.86	5.00	0.17	5.92	0.58	4.53	2.34	6.54	1.02	4.47	0.90
	2	11.64	2.11	8.93	1.43	13.56	1.57	9.34	2.76	13.19	1.50	10.41	2.60
K_d	32	2.10	0.17	2.41	−0.43	2.25	0.39	1.25	−0.19	3.16	0.12	1.22	0.05
	8	11.72	2.45	9.92	0.87	13.13	2.08	10.12	5.20	17.28	3.46	6.46	1.23
	2	29.52	6.42	26.06	6.62	31.43	9.98	14.15	5.66	40.96	8.36	15.52	4.51
R	32	1.18	−0.04	1.21	0.24	1.29	−0.18	0.86	0.06	1.44	−0.09	0.93	0.01
	8	5.60	−0.29	5.30	0.43	6.01	−0.22	4.35	−1.96	6.81	−0.17	4.47	−0.42
	2	11.83	0.45	9.03	0.28	13.69	1.29	9.82	−1.31	13.25	1.21	10.02	−0.55
Q_n	32	0.12	−0.02	0.11	−0.01	0.12	−0.02	0.13	−0.01	0.14	−0.02	0.10	−0.01
	8	0.79	0.07	0.60	0.11	0.85	0.15	0.74	−0.30	0.93	0.13	0.65	0.03
	2	1.56	0.04	1.19	0.18	1.72	0.01	1.42	−0.31	1.67	0.06	1.47	−0.04
L_{WN}	32	0.17	0.02	0.14	0.02	0.18	0.03	0.19	0.02	0.21	0.03	0.14	0.01
	8	1.00	−0.12	0.85	−0.10	1.06	−0.18	1.04	0.14	1.21	−0.09	0.82	−0.11
	2	2.32	0.08	1.75	−0.12	2.58	0.20	2.39	0.34	2.45	−0.01	2.23	0.17
$\check{L}_{WN}$	32	1.22	−0.06	1.23	0.25	1.35	−0.18	0.88	0.06	1.49	−0.10	0.95	0.03
	8	5.70	−0.35	5.28	0.45	6.27	−0.21	4.52	−1.94	6.97	−0.21	4.58	−0.48
	2	12.14	0.39	8.96	0.10	14.30	1.52	10.28	−1.35	14.01	1.52	10.73	−0.12

In fact, on these conditions the increase in sea state is not accompanied by wave breaking and a consequent reduction in wave perturbations, and should lead to an increase of the uncertainties on wind speed decrease. For high sea state ($S_s = 3$) the present dataset has shown that the uncertainties significantly increase as a function of wind speed W_s. At $S_s = 3$, for $W_s < 5$ m s^{-1} the $|\psi|$ value related to $E_d(0^-, \lambda)$ for $N = 2$ decreases to 7.6% (determined from 20 profiles), and with $W_s \geq 5$ m s^{-1} it increases up to 10.2% (determined from 21 profiles). This apparently contradictory result is potentially due to the poor characterization of wave height through the applied sea state code, added to the low occurrence of large regular waves at the coastal site.

The uncertainty analysis as a function of $K_d(\lambda)$ at $\lambda = 490$ nm shows a general decrease in $|\psi|$ values as $K_d(490)$ increases. This is in agreement with an intuitive decrease of wave-induced perturbations with light attenuation. Within the primary quantities, the largest perturbations due to the $K_d(490)$ change are again observed for $K_d(\lambda)$ and $E_d(0^-, \lambda)$. Specifically, with $N = 2$ the $|\psi|$ values for $K_d(\lambda)$ drop from 41.0% for the subset of profiles characterized by $K_d(490) < 0.14$ m^{-1}, down to 15.5% for the subset of profiles characterized by $K_d(490) \geq 0.14$ m^{-1}. The corresponding $|\psi|$ values for $E_d(0^-, \lambda)$ are much lower and show values of 13.2% and 10.4%, respectively.

The $|\psi|$ values computed for $L_{WN}(\lambda)$, as expected, are close to those of $L_u(0^-, \lambda)$. The $|\psi|$ values computed for $R(\lambda)$ and $\check{L}_{WN}(\lambda)$ are generally close to the highest $|\psi|$ values of the related primary quantities, that is, $E_d(0^-, \lambda)$. On the other hand, the $|\psi|$ values computed for $Q_n(\lambda)$ exhibit values close to those of $L_u(0^-, \lambda)$ and lower than those of $E_u(0^-, \lambda)$. This suggests the existence of correlations between perturbations affecting the analyzed $L_u(0^-, \lambda)$ and $E_u(0^-, \lambda)$ values.

The increase of uncertainties in $\check{L}_{WN}(\lambda)$ computed with $E_d(0^-, \lambda)$ values extrapolated above the sea surface is relevant, with respect to uncertainties in $L_{WN}(\lambda)$ computed with above-water $E_d(0^+, \lambda)$ values collected from a stable platform not subject to waves motion. This result fully supports the recommendations of using above-water $E_d(0^+, \lambda)$ measurements—when not significantly affected by the motion of the deployment platform (i.e., ship or buoy)—to increase the accuracy in the normalized water-leaving radiances (Zaneveld et al. 2001).

An alternative to the analysis of wave-induced perturbations previously discussed as a function of sea state and of seawater diffuse attenuation coefficient is the use

TABLE 6. Spectral average uncertainties (%) for $N = 16$ as a function of the statistical dispersion of the profile data given by the standard deviation σ_d (see text); M indicates the number of profiles used for each analysis.

	All ($M = 244$)		$\sigma_d < 0.15$ ($M = 120$)		$\sigma_d \geq 0.15$ ($M = 124$)	
	$\lvert\psi\rvert$	ψ	$\lvert\psi\rvert$	ψ	$\lvert\psi\rvert$	ψ
L_u	0.55	0.01	0.48	−0.03	0.62	0.07
E_u	0.31	0.01	0.29	−0.01	0.34	0.04
E_d	3.06	0.20	2.14	−0.21	3.84	0.49
K_d	5.94	0.24	3.20	−0.28	8.90	0.95

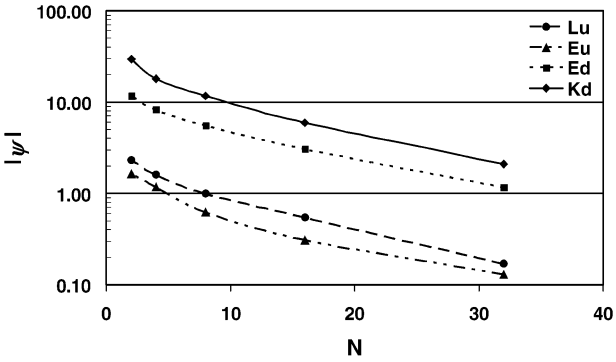

FIG. 4. Spectral average $|\psi|$ values, as a function of N, for the primary optical quantities $L_u(0^-, \lambda)$, $E_u(0^-, \lambda)$, $E_d(0^-, \lambda)$, and $K_d(\lambda)$.

of statistics describing fluctuations of the light signal in the extrapolation interval. An analysis solely based on the standard deviation σ_d of differences between the log-transformed $E_d(z, 490)$ data and their fit in the extrapolation interval is summarized in Table 6 for profiles characterized by 16 measurements per meter [a depth resolution achievable with the current advanced profilers (Hooker et al. 2003)]. As expected, the uncertainties increase as σ_d increases. This suggests that the statistics describing the fluctuations of the light signal in the extrapolation interval could be used to define an uncertainty index for subsurface optical values alternative to quantities describing waves and seawater optical properties.

b. Depth resolution requirements

The spectral average $|\psi|$ values for the primary optical quantities are plotted in Fig. 4 as a function of N. The almost exponential dependence of $|\psi|$ on N is explained by the fact that these uncertainties result from the difference in quantities determined from exponential fits. Curves like those plotted in Fig. 4 can be used to estimate the depth resolution required to convey wave-induced uncertainties below a predefined threshold. Setting the threshold to 2% for each primary quantity, a value comparable to the absolute calibration uncertainties, the depth resolution requirements determined from curves of $|\psi|$ are given in Table 7 at 443, 555, and 665 nm for in-water optical profiles taken with $K_d(490) < 0.14\ \text{m}^{-1}$ and $S_s = 2$ (those affected by the largest wave perturbations). For completeness, estimated depth resolutions are also provided for the 1% and 5% thresholds. Data show values varying for each primary quantity as a function of wavelength. Specifically, the 2% target (boldface values), for the 443–665-nm spectral range, requires depth resolutions higher than 11, 40, 3, and 2 cm for $L_u(0^-, \lambda)$, $E_u(0^-, \lambda)$, $E_d(0^-, \lambda)$, and $K_d(\lambda)$, respectively. By restricting the uncertainty below 1%, the depth resolutions increase up to 5, 13, 2, and 2 cm, respectively. Conversely, by relaxing the uncertainty threshold to 5%, the depth resolutions decrease to values higher than 50 cm for $L_u(0^-, \lambda)$, $E_u(0^-, \lambda)$, and to 6 and 3 cm for $E_d(0^-, \lambda)$ and $K_d(\lambda)$, respectively. The former values confirm that the primary optical quantities determined from full-resolution WiSPER data with depth resolution better than 1.6 cm are not significantly affected by wave-induced perturbations [i.e., they are negligible in $L_u(0^-, \lambda)$ and $E_u(0^-, \lambda)$, and less than 1% in $E_d(0^-, \lambda)$ and $K_d(\lambda)$]. This helps in evaluating the overall uncertainty budget in subsurface quantities determined from profiles collected in coastal waters under environmental conditions similar to those encountered at the AAOT using systems having an acquisition rate and optics similar to those of WiSPER. Specifically, the data in Table 7 suggest that the uncertainties determined with profiles collected under the stated environmental conditions with current advanced free-fall systems (having an acquisition rate of 6 Hz, a deployment speed of $\sim 0.25\ \text{m s}^{-1}$, and the same optics as in WiSPER) are lower than 1% for $L_u(0^-, \lambda)$ and $E_u(0^-, \lambda)$, and of the order of 2% for $E_d(0^-, \lambda)$. For $K_d(\lambda)$ the uncertainties are close to 5% in the 412–555-nm interval and of the order of 2% in the red.

TABLE 7. Depth resolution requirements (cm) ensuring 1%, 2%, and 5% uncertainty values in primary optical quantities.

λ	443			555			665		
Uncertainty (%)	1	**2**	5	1	**2**	5	1	**2**	5
L_u	17	**50**	>50	13	**33**	>50	5.3	**11**	**50**
E_u	50	>**50**	>50	25	>**50**	>50	13	**40**	>**50**
E_d	3.0	**4.4**	10	2.9	**3.5**	6.3	2.4	**3.3**	**6.3**
K_d	2.1	**2.6**	3.9	1.8	**2.1**	2.9	2.6	**3.7**	**9.1**

c. Applicability of the proposed depth resolution requirements

The results from this study suggest that in coastal waters the wave-induced uncertainties can be reduced below 2% with the number of measurements per meter higher than approximately 9, 3, 33, and 50 for $L_u(0^-, \lambda)$, $E_u(0^-, \lambda)$, $E_d(0^-, \lambda)$, and $K_d(\lambda)$, respectively. These values are much more restrictive than the ''at least 2, and preferably 6 to 8 measurements per meter'' given in the ocean optics protocols (Mueller 2003) for optically deep waters and assuming the extrapolation interval to be equal to at least one optical depth. This difference in requirements between coastal and oceanic optical profiles highlights the superior technological needs for the former ensuring the capability of sampling with higher depth resolution and of acquiring data as close as possible to the surface to maximize the extrapolation interval in the presence of highly inhomogeneous water columns. This suggests that, when profilers do not meet the given requirements, alternative methods should be searched. A practical solution is to add data from successive casts (Zaneveld et al. 2001; D'Alimonte et al. 2001) to produce a single profile with a higher depth resolution. An attempt to experimentally verify this method was made using the JRC version of the miniature National Aeronautics and Space Administration (NASA) Environmental Sampling System (JRC-miniNESS). This free-fall profiler has the same acquisition rate and radiometers as does WiSPER (Hooker et al. 2003). The dataset used for the verification included 58 fully independent measurement sequences, each composed of five consecutive profiles collected within 10 min during clear-sky and stable illumination conditions in the vicinity of the AAOT with a deployment speed of $\sim$1 m s^{-1}. When combining the data of the consecutive profiles for each measurement sequence and thus increasing the number of samples from $\sim$6 to $\sim$30 per meter, the comparison of primary optical quantities determined from the single midsequence profile versus the multicast profile data showed spectral average $|\psi|$ values of 1.7%, 2.7%, 5.8%, and 14.6% for $L_u(0^-, \lambda)$, $E_u(0^-, \lambda)$, $E_d(0^-, \lambda)$, and $K_d(\lambda)$, respectively. These uncertainties compare in magnitude with the values of 1.0%, 0.6%, 5.2%, and 11.8% resulting from the fully independent comparison of WiSPER reduced resolution profiles with 8 and 32 samples per meter. The differences between the results obtained with the JRC-miniNESS and the reduced resolution WiSPER data are mostly justified by (a) the environmental variability affecting the successive profiles from the free-fall and canceling out in the WiSPER data, (b) tilt effects present in the free-fall and not in the WiSPER data, (c) slight differences in the free-fall and WiSPER depth resolutions used for the comparison, and finally (d) the mutual positions of radiometers with respect to each other in the two profiling systems. A peculiar case in the former analysis of multicast profile data is encountered with $E_u(0^-, \lambda)$ exhibiting a higher $|\psi|$ value than that of $L_u(0^-, \lambda)$. This can be explained by the position of the E_u sensor, installed on the nose of the JRC-miniNESS at approximately 0.9 m below the L_u and E_d sensors (Hooker et al. 2003). Because of the adoption of a common extrapolation interval for the processing of $L_u(z, \lambda)$, $E_u(z, \lambda)$, and $E_d(z, \lambda)$, the determination of $E_u(0^-, \lambda)$ must rely on a smaller effective extrapolation layer. Thus, the increase in depth resolution through the multicast approach produces a more significant improvement in the accuracy of $E_u(0^-, \lambda)$ than in that of $L_u(0^-, \lambda)$, determined from these specific free-fall profile data.

In conclusion, the former analysis based on free-fall data confirms the possibility of appreciably reducing the wave-induced perturbations through the multicast approach and it also indirectly confirms the appropriateness of the uncertainty analysis produced with the full and reduced resolution WiSPER data. Finally, when considering the depth resolution requirements suggested by the present study, it must be remembered that they do not apply to data taken with profilers characterized by optics and a sampling frequency that is much different than those of WiSPER. For instance, profilers based on hyperspectral sensors whose measurements are characterized by a quite long acquisition period deserve specific investigations.

6. Conclusions

The analysis of $L_u(z, \lambda)$, $E_u(z, \lambda)$, and $E_d(z, \lambda)$ optical profiles taken in coastal waters confirmed the relevance of wave effects in the determination of spectral primary and derived subsurface optical quantities. Wave-induced uncertainties, independent from the accuracy of absolute calibration; corrections for shading perturbations; and changes in seawater and illumination conditions were estimated by comparing values of the considered quantities computed from decreased resolution profiles (2–32 measurements per meter) with values computed from full-resolution profiles (64 measurements per meter). The primary quantities $E_d(0^-, \lambda)$ and $K_d(\lambda)$, and the derived quantities computed with $E_d(0^-, \lambda)$, showed the largest uncertainties due to wave focusing and defocusing.

The analysis of perturbations as a function of sea state showed values increasing for wave heights varying from 0.0–0.1 to 0.1–0.5 m, and generally decreasing with wave heights of 0.5–1.25 m. The decrease is attributed to an increase in the in-water diffuse light field due to the superimposition of different waves in addition to wave breaking effects.

The analysis of wave perturbations as a function of $K_d(490)$ confirmed an expected increase in uncertainties as $K_d(490)$ decreases, in agreement with a less diffuse light field.

Setting different maximum uncertainty thresholds for wave-induced perturbations in primary quantities, the

depth resolution requirements significantly vary as a function of wavelength for the typical measurement conditions characterizing the dataset. For a 2% uncertainty threshold, within the 443–665-nm spectral range, with $K_d(490) < 0.14\ \mathrm{m}^{-1}$, a wave height of 0.1–0.5 m, average extrapolation intervals of 0.4–3.6 m, an acquisition rate of 6 Hz, a 20° full angle field of view for radiance sensors, and ~1-cm diameter of irradiance collectors, the required minimum depth resolutions are 11, 40, 3, and 2 cm for $L_u(0^-, \lambda)$, $E_u(0^-, \lambda)$, $E_d(0^-, \lambda)$, and $K_d(\lambda)$, respectively. These results are a first attempt at quantifying wave perturbation uncertainties in subsurface optical quantities from optical profile data taken in coastal waters. It is recognized that the estimated uncertainties cannot be applied to any water type or any commercial instrument. However, due to the number of different conditions analyzed in the study, they can still be of use in the estimation of the overall uncertainty budget of primary optical quantities computed from radiometric profile data taken in coastal waters.

General conclusions—supported by the quantitative results produced within the uncertainty analysis—highlight that in coastal areas, where the extrapolation depth could be restricted to a few meters just below the surface, the determination of accurate subsurface primary and derived quantities needs the following:

1) profiling with depth resolutions satisfying requirements varying significantly as a function of wavelength, seawater optical properties, and sea state; and
2) computing the normalized water-leaving radiance $L_{WN}(\lambda)$, preferring the above-water $E_d(0^+, \lambda)$ measurements (when not affected by significant ship or buoy motion) to the $E_d(0^-, \lambda)$ extrapolated above the sea surface.

Finally, a complete reduction of wave-induced perturbations in the spectral ratios of primary and derived quantities, with respect to single spectral quantities, can only be effective when a single collector or field of view is used to simultaneously gather the light for all spectral channels.

Acknowledgments. The current work has been supported through NASA Grant NCC5-371 and the JRC Coastal Water Monitoring program. A particular acknowledgment is due to Dirk van der Linde for the extensive participation in the collection of WiSPER data within the framework of the CoASTS measurement campaigns. Acknowledgments are also due to the anonymous reviewers for the detailed revisions that led to an improvement of the original work.

REFERENCES

Antoine, D., and P. Guevel, 2000: Calibration and validation of satellite ocean color observations: The BUSSOLE project. *Proc. Ocean Optics XV,* Monaco, Office of Naval Research, CD-ROM. [Available from the Office of Naval Research, BCT1, 800 North Quincy St., Arlington, VA 22217-5660.]

Berthon, J.-F., G. Zibordi, J. P. Doyle, S. Grossi, D. van der Linde, and C. Targa, 2002: Coastal Atmosphere and Sea Time Series (CoASTS), Part 2: Data analysis. NASA Tech. Memo. 206892, Vol. 20, S. B. Hooker and E. R. Firestone, Eds., NASA Goddard Space Flight Center, 25 pp.

Clark, D. K., H. R. Gordon, K. J. Voss, Y. Ge, W. Broenkow, and C. Trees, 1997: Validation of atmospheric correction over the oceans. *J. Geophys. Res.,* **102,** 17 209–17 217.

D'Alimonte, D., G. Zibordi, and J. F. Berthon, 2001: The JRC processing system. NASA Tech. Memo. 206892, Vol. 15, S. B. Hooker and E. R. Firestone, Eds., NASA Goddard Space Flight Center, 56 pp.

Dera, J., and J. Olszewski, 1978: Experimental study of short period irradiance fluctuations under an undulated sea surface. *Oceanologia,* **10,** 27–49.

——, and D. Stramski, 1986: Maximum effects of sunlight focusing under a wind-disturbed sea surface. *Oceanologia,* **23,** 15–42.

——, S. Sagan, and D. Stramski, 1993: Focusing of sunlight by the sea surface waves: New results from the Black Sea. *Oceanologia,* **34,** 13–25.

Dierssen, H. M., and R. C. Smith, 1996: Estimation of irradiance just below the air–water interface. *Proc. SPIE,* **2963,** 204–209.

Doyle, J. P., and G. Zibordi, 2002: Optical propagation within a 3-dimensional shadowed atmosphere–ocean field: Application to large deployment structures. *Appl. Opt.,* **41,** 4283–4306.

——, S. B. Hooker, G. Zibordi, and D. van der Linde, 2003: Tower perturbation measurements in in-water radiometry. NASA Tech. Memo. 2002-206892, Vol. 25, S. B. Hooker and E. R. Firestone, Eds., NASA Goddard Space Flight Center, 33 pp.

Hooker, S. B., and W. E. Esaias, 1993: An overview of the SeaWiFS project. *Eos, Trans. Amer. Geophys. Union,* **74,** 241–246.

——, and S. Maritorena, 2000: An evaluation of oceanographic radiometers and deployment methodologies. *J. Atmos. Oceanic Technol.,* **17,** 811–830.

——, G. Zibordi, D. van der Linde, D. D'Alimonte, J.-F. Berthon, and J. Brown, 2003: Tower perturbation measurements in above-water radiometry. NASA Tech. Memo. 2002-206892, Vol. 23, S. B. Hooker and E. R. Firestone, Eds., NASA Goddard Space Flight Center, 35 pp.

Loisel, H., and A. Morel, 1998: Light scattering and chlorophyll concentration in Case-1 waters: A reexamination. *Limnol. Oceanogr.,* **43,** 847–858.

Mobley, C. D., 1994: *Light in the Water.* Academic Press, 592 pp.

Mueller, J. L., 2003: Overview of measurement and data analysis methods. NASA Tech. Memo. 2003-211621, Rev. 4, Vol. III, J. L. Mueller, G. S. Fargion, and C. R. McClain, Eds., NASA Goddard Space Flight Center, 7–20.

——, and R. W. Austin, 1995: Ocean optics protocols for SeaWiFS validation. NASA Tech. Memo. 104566, Vol. 25, S. B. Hooker and E. R. Firestone, Eds., NASA Goddard Space Flight Center, 66 pp.

O'Reilly, J. R., S. Maritorena, B. G. Mitchell, D. A. Siegel, K. L. Carder, S. A. Garver, M. Kahru, and C. McClain, 1998: Ocean color chlorophyll algorithms for SeaWiFS. *J. Geophys. Res.,* **103,** 24 937–24 953.

Pinkerton, M. H., and J. Aiken, 1999: Calibration and validation of remotely sensed observations of ocean color from a moored data buoy. *J. Atmos. Oceanic Technol.,* **16,** 915–923.

Schenck, H., 1957: On the focusing of sunlight by ocean waves. *J. Opt. Soc. Amer.,* **47,** 653–657.

Smith, R. C., and K. S. Baker, 1984: The analysis of the ocean optical data. *Proc. SPIE,* **489,** 119–126.

Snyder, R. L., and J. Dera, 1970: Wave-induced light-field fluctuations in the sea. *J. Opt. Soc. Amer.,* **60,** 1072–1079.

Stramski, D., and J. Dera, 1988: On the mechanism for producing flashing light under a wind disturbed water surface. *Oceanologia,* **25,** 5–21.

Walker, R. E., 1994: *Marine Light Field Statistics.* Wiley, 675 pp.

Weidemann, A., R. Hollman, M. Wilcox, and B. Linzell, 1990: Calculation of near surface attenuation coefficients: The influence of wave focusing. *Proc. SPIE,* **1302,** 492–504.

WMO, 1983: *Guide to the Meteorological Instruments and Methods of Observation.* WMO-8, 517 pp.

Zaneveld, J. R., V. E. Boss, and A. Barnard, 2001: Influence of surface waves on measured and modeled irradiance profiles. *Appl. Opt.,* **40,** 1442–1449.

Zibordi, G., and G. M. Ferrari, 1995: Instrument self shading in underwater optical measurements: Experimental data. *Appl. Opt.,* **34,** 2750–2754.

——, J. P. Doyle, and S. B. Hooker, 1999: Offshore tower shading effects on in-water optical measurements. *J. Atmos. Oceanic Technol.,* **16,** 1767–1779.

——, J.-F. Berthon, J. P. Doyle, S. Grossi, D. van der Linde, C. Targa, and L. Alberotanza, 2002: Coastal Atmosphere and Sea Time Series (CoASTS), Part 1: A long-term measurement program. NASA Tech. Memo. 206892, Vol. 19, S. B. Hooker and E. R. Firestone, Eds., NASA Goddard Space Flight Center, 29 pp.

——, S. B. Hooker, J. Mueller, and G. Lazin, 2004: Characterization of the immersion coefficient of a class of underwater irradiance sensors. *J. Atmos. Oceanic Technol.,* **21,** 501–514.